

## CHAPTER - II

### STUDY AREA

#### 2.1. Mandovi Estuary

##### 2.1.1. Introduction

The Mandovi estuary is a well mixed coastal plain estuary situated between  $15^{\circ} 27'$  to  $15^{\circ} 31'N$  and longitude  $73^{\circ} 45'$  to  $73^{\circ} 59'E$  in Goa along the west coast of India (Fig. 2.1). Along with the adjacent Zuari estuary, it is one of the better studied estuarine systems in the country (Qasim & Sen Gupta, 1981; Qasim, 2003; De Souza, 1983; Devassy & Goes, 1988). The river has its source in the Western Ghats and runs  $\sim 75$  km through the state of Goa before meeting the Arabian Sea. The estuary covers an area of  $\sim 29$  km<sup>2</sup> and its width increases from 0.25 km at the head to 3.2 km at the mouth. The depth of the estuary varies from 8-10m at the mouth to  $< 2$ m at the fresh water end. The average depth of the estuary is  $\sim 4$ m.

The estuary remains tide dominated during the dry season (October-May) as rainfall and freshwater inflow remain negligibly low and saline water intrudes up to nearly 55 km upstream. However during the southwest monsoon season (June-September) Goa receives an average rainfall of 3000 mm of which 80% occurs in the first three months (June-August). As a result, the estuary receives a large amount of fresh water through land run off from its catchment area of 1150 km<sup>2</sup> including forested land. The estuary is connected to the Zuari estuary by the man made Cumbarjua canal which is located 14 km and 11 km away from the mouths of Mandovi and Zuari estuaries respectively. The canal is about 17 km in length and 0.5 - 0.7 km in width.

The estuary remains navigable round the year up to 45 km upstream from the mouth and is one of the two main waterways in Goa for transporting iron ore by barges. However, during the monsoon period, navigation is suspended in the Mandovi estuary because of the formation of shoals or sand bars near the estuary mouth. These shoals are popularly

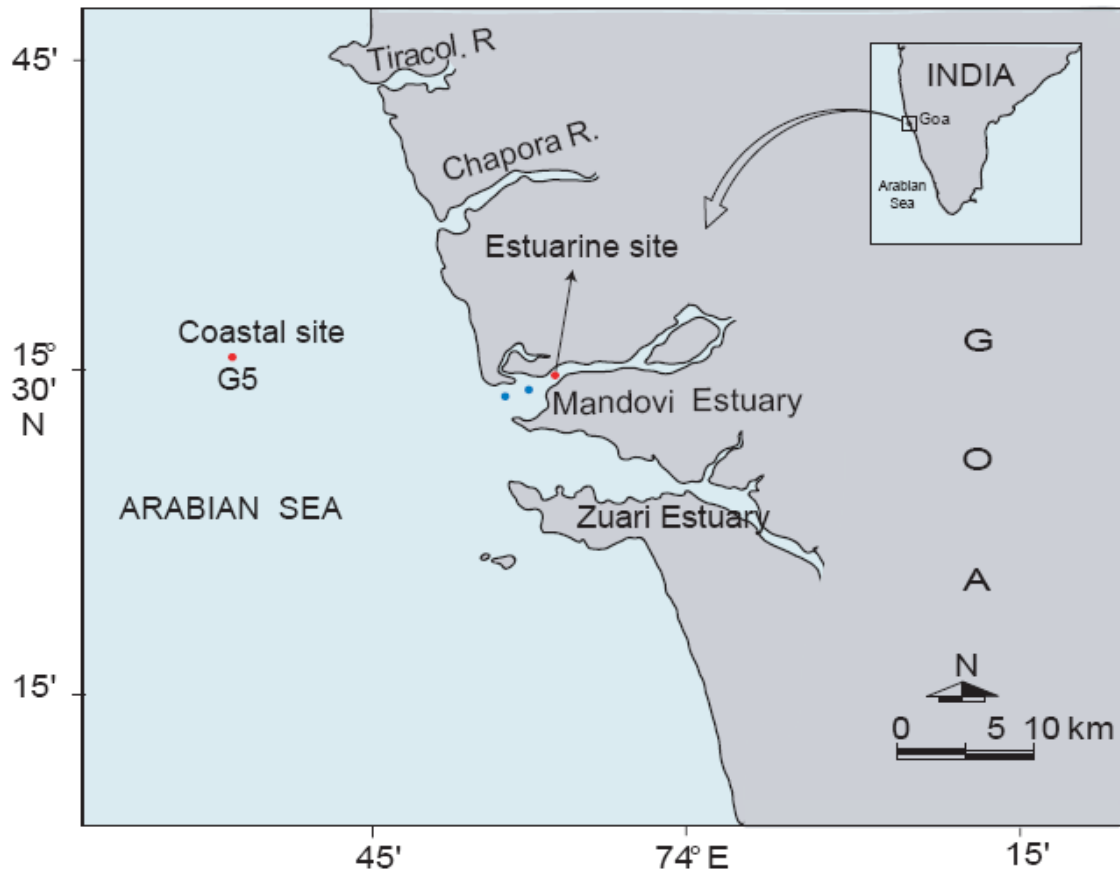


**Fig. 2.1:** Geographical location of the Mandovi estuary and the coastal station.

Red points are the sites where benthic flux was measured.

known as the Aguada bar and the Reis Magos bar; the former occurs in the Aguada Bay and the latter is located opposite to the old Portuguese fort of Reis Magos.

The estuary remains well mixed throughout the year except during the monsoon when a vertical stratification appears (Verma *et al.*, 1975) because of heavy freshwater flow in the surface layer and seawater penetration in the bottom layer. The lower saline layer moves up and down with the tide in the form of a salt wedge some distance from the estuary mouth.

The catchment area of the estuary is densely populated. However, since the villages are not connected to any sewage system, no waste load apparently enters the estuary from these areas directly, but treated waste from the sewage system of Panjim city is discharged at Campal (3 km from the mouth).

### **2.1.2. Hydrography**

Hydrographic features of the estuary were investigated as early as in 1969 when studies were undertaken on the changes in some environmental features in relation to the tidal cycle (Dehadrai, 1970). The rate of primary production and chlorophyll-a concentration were found to be regulated by flood and ebb tides. Maximum current speeds during the flood and ebb were 160 and 108 cm/s respectively. During the southwest monsoon, the discharge of a large volume of fresh water ( $13.96 \times 10^5 \text{ m}^3 \text{ d}^{-1}$ ) into the estuary has been found to increase the effect of ebb and controls the flow of flood. Murty & Das (1972) observed the variation of salinity with the tide in the estuary. Phytoplankton pigments in the estuary reach peak values in the premonsoon season (March-May) and minimum during the monsoon (June-September). Variations in the hydrographic conditions are minimal during the premonsoon season. Suspended matter has been reported to be higher in the middle part and upstream of the estuary than at the mouth because of stronger tidal currents in the middle and upstream portions (Cherian *et al.*, 1974).

#### **2.1.2.1. Tidal Propagation**

The estuary experiences tides of semi-diurnal type with a range between 2 and 2.3m. The speed of the propagation of both diurnal and semidiurnal tides was found to be 6m/s. The amplitude of the semidiurnal band was the largest of all the constituents and remains almost similar in both dry and wet seasons (Shetye *et al.*, 1995). The tidal amplitude and phase remain unchanged up to about 40 km from the estuary mouth and then undergo abrupt decreases over the next 10 km (Shetye *et al.*, 1995). This decay in tidal amplitude is even more rapid during the period of higher river runoff.

#### **2.1.2.2. Temperature**

Temperature of the estuarine water shows a pronounced seasonal variation, increasing steadily from January to May, followed by a sharp decrease in the monsoon period owing to heavy precipitation and decrease in solar radiation. It increases again in the post monsoon season (Fig. 2.2a). Temperature in the estuary varies between 25 and 31.5°C attaining its maximum in April-May and minimum in June-July.

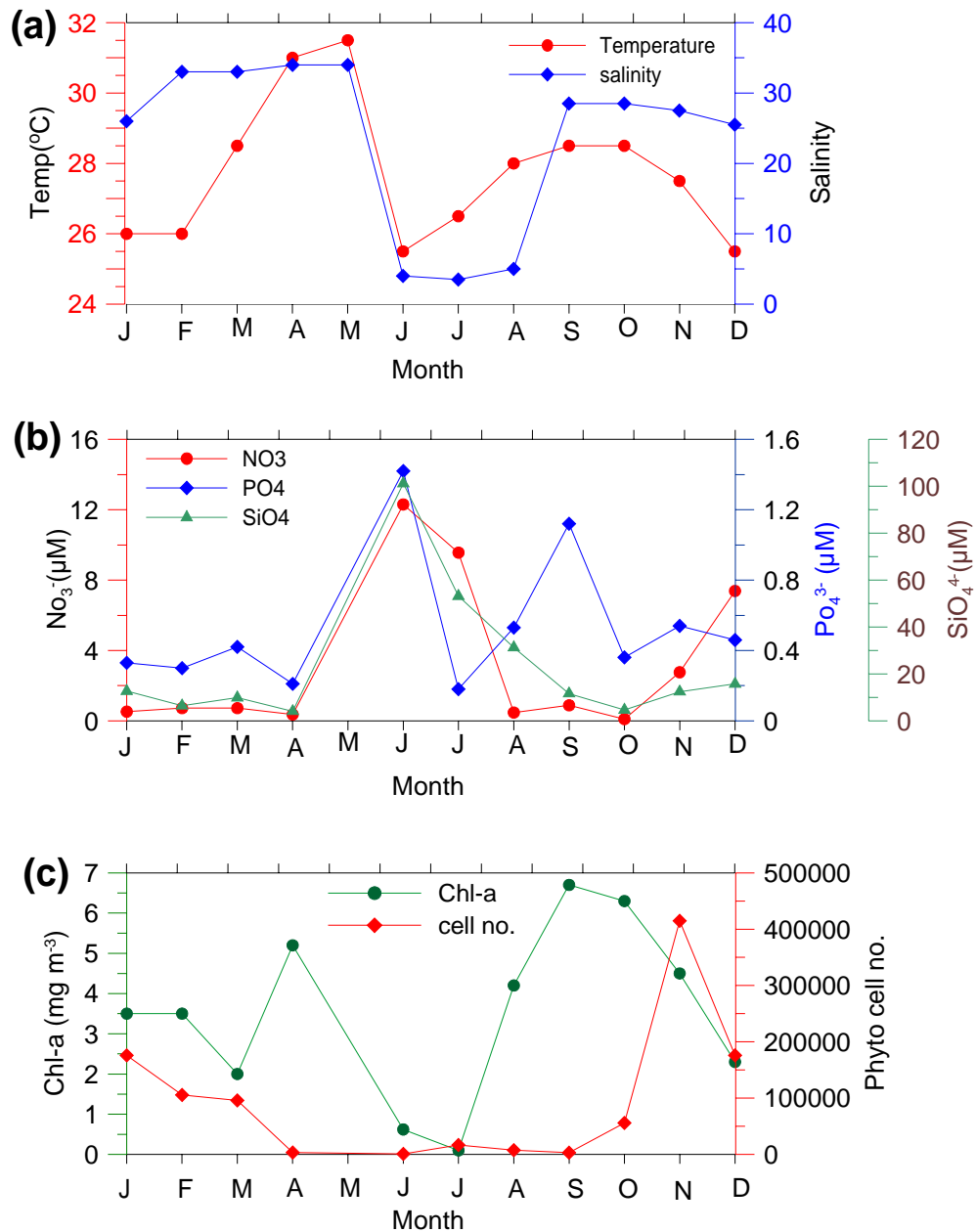


**Fig.2.2:** Seasonal variation of physico-chemical and biological parameters in Mandovi estuary.

### 2.1.2.3. Salinity

Salinity in the estuary undergoes large variability mainly because of tidal influence in non-monsoon seasons and freshwater inflow in the monsoon season. Salinity in dry season varies between 25.0 and 34.0 attaining its maximum (33.0 - 34.0) in April-May but decreases sharply (4.0) in June (Fig. 2.2a) following the onset of precipitation and

heavy riverine flow. In the premonsoon period, the estuary becomes an extension of the sea and saline water penetrates upstream as far as 55 km from the mouth. It behaves almost like a freshwater body from June to August due to massive freshwater inflow. After August, decreasing rainfall and consequently increasing tidal dominance again increases the salinity of the estuarine water. Previous studies by Qasim and Sen Gupta (1981) also showed a similar seasonal variation.

The estuarine water column is well mixed during the non-monsoon periods when the fresh water runoff is low. However, during the monsoon season, because of the formation of salt wedge, the water column becomes stratified 2-3m below the surface. The salt-wedge persists up to a distance 10 km from the mouth during peak monsoon period. During this period while fresh water dominates the upper water column, seawater with varying salinity of 2.50 to 15.00 is found at the bottom (Qasim and Sen Gupta, 1981). The rest of the estuary remains filled with fresh water with practically no salt water intrusion anywhere. Immediately after the monsoon, partial mixing of saline and fresh water occurs, but some stratification continues to persist at few places in the estuary (Murty & Das, 1972). In the premonsoon season, on the other hand, no stratification is found anywhere and the water column remains well mixed and salt water penetrates upstream, as stated earlier.

### **2.1.3. Biogeochemical parameters**

#### **2.1.3.1. Dissolved Oxygen**

Oxygen concentration in the estuarine water varies during the tidal cycle; decreasing with rising tide and increasing with the falling tide (Qasim, 2003) which is because of higher solubility of oxygen in fresher water compared to seawater. Uniform oxygen concentration is found in the estuary from surface to bottom during pre- and postmonsoon seasons when the water column remains well mixed. However, during the monsoon season because of the prevailing vertical stratification in the water column, high oxygen values are found at the surface with low concentration found close to the bottom. Dissolved oxygen varies from 4 to 5 ml L<sup>-1</sup> in the pre- and postmonsoon seasons and remains generally high (5-6 ml L<sup>-1</sup>) during the monsoon season (Qasim & Sen Gupta, 1981) (Fig. 2.3) because of the dominance of fresh water in the estuary.

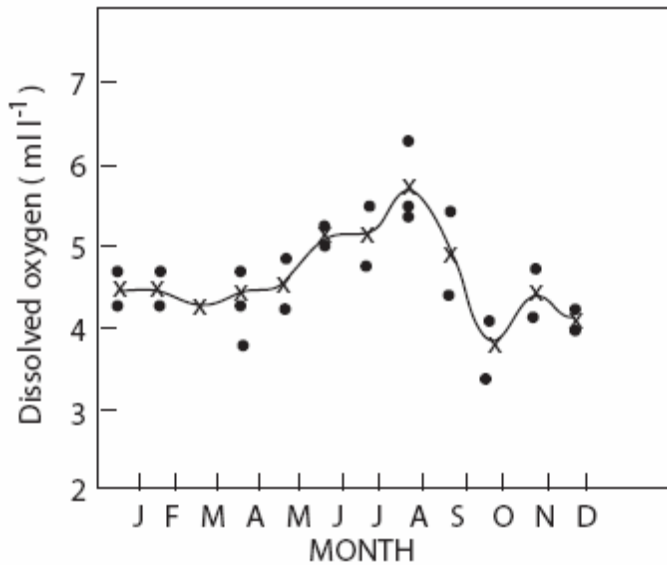


**Fig. 2.3:** Seasonal variation of dissolved oxygen in the Mandovi Estuary (Qasim & Sen Gupta, 1981).

#### 2.1.3.2. Nutrients

In the premonsoon season, concentrations of nitrate, phosphate and silicate are generally low as a result of high biological uptake as the clear water column and increased solar radiation favor photosynthesis. The river remains the major source of nutrients to the estuary. The estuary is usually enriched with nutrients in the monsoon season (Fig. 1b) owing to increased riverine discharge and land runoff. Silicate exceeds 100  $\mu\text{M}$  in the monsoon season which is an indicator of strong river influence. Atmospheric precipitation has also been reported to contain considerable amount of  $\text{NH}_4^+$  and  $\text{NO}_3^-$  (Sen Gupta, 1973). However, since greater cloud cover and turbidity reduce primary production considerably these nutrients are not utilized and are transported to the sea (Fig. 2.4). After the monsoon, conditions become favorable for algal uptake of nutrients which leads to a decrease in nutrient concentration. Local land runoff occasionally increases nutrient concentration towards the end of the year. Unlike  $\text{NO}_3^-$ , phosphate never becomes depleted in the estuarine water because of its adsorption and desorption on to suspended particles and sediment (Pomeroy *et al.*, 1965).

### 2.1.3.3. Phytoplankton and Primary productivity

The Mandovi estuary has been found to be inhabited by 82 species of phytoplankton of which 63 are diatoms, 14 dinoflagellates, 3 blue green algae and 2 green algae (Devassy & Bhargava, 1978). Diatoms are by far the dominant group throughout the year, except in September when dinoflagellates sometimes contribute up to 77.6% to the total algal biomass. Diatoms remain the most successful group in the estuary even at low salinities (<1‰). The estuarine diatoms tolerate a wide range of salinity (2.5-31.5) while dinoflagellates form blooms at salinities between 25.5 and 31.8. (Devassy and Goes, 1988)

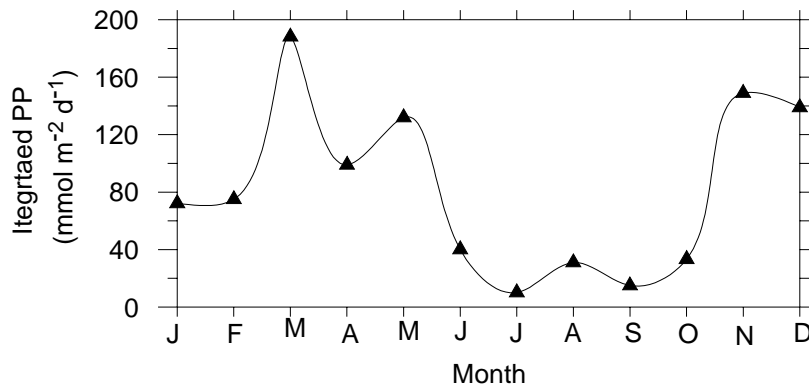


**Fig. 2.4:** Seasonal variation in depth integrated primary production in the Mandovi estuary (Pradeep Ram *et al.*, 2003).

Primary production is the highest in the premonsoon (March-May) and post monsoon seasons (October-November) owing to high transparency of the water column and increased solar radiation. Following heavy rainfall from June onwards, enormous volume of freshwater, through land runoff and river discharge, brings about extensive dilution, stratification in the water column and salt wedge formation, and high turbidity in the estuary. During this period, phytoplankton density and diversity are the lowest, in spite of nutrients which remain largely unutilized. Due to high turbidity and cloud cover, light penetration to the water column is minimal which results in low phytoplankton crop. Towards the end of monsoon, there is progressive increase in salinity and with return of clear water conditions, phytoplankton blooms develop. Thus, a gradual repopulation of

phytoplankton crop occurs during the postmonsoon period, which is maintained in subsequent months (Devassy & Goes, 1988).

#### 2.1.3.4. Benthic Fauna

Parulekar and Dwivedi (1974) found dense population of clams, bivalves, polychaetes and crustaceans in the estuarine sediment. Later studies by Ansari *et al.* (1986) and Ansari & Parulekar (1993) revealed that the estuarine sediment is inhabited by a wide variety of benthic organisms whose population varies with season and location.

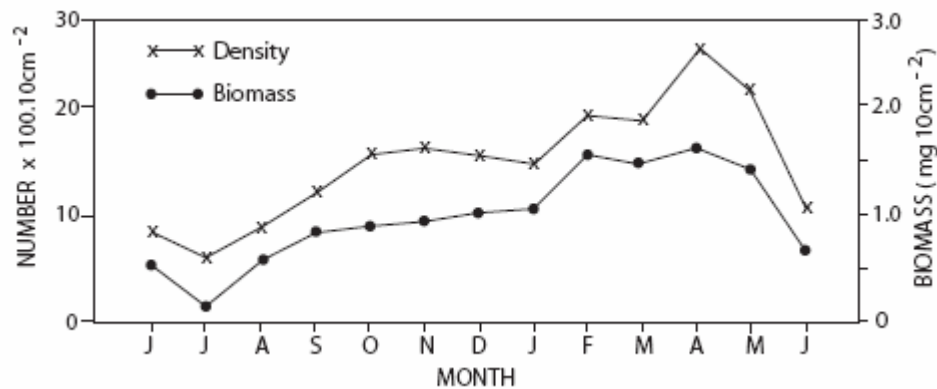


**Fig. 2.5:** Seasonal variation in abundance of total meiofauna in the the sediment of the Mandovi Estuary (Ansari & Parulekar, 1993).

These authors reported the presence of 69 species of benthic organisms including nematodes, copepods, polychaetes, turbellarians and ostracods. Faunal abundance was reported to be mainly controlled by salinity and temperature. Population decreased with increasing distance from the estuary mouth. The densities of copepods, polychaetes and turbellarians were higher during the pre- and postmonsoon periods. Maximal density (2425/ m<sup>2</sup>) was observed during the high salinity season (premonsoon) and the lowest population (650/ m<sup>2</sup>) was observed in the low salinity period (monsoon) (Fig. 2.5). This showed low tolerance of most species of benthic organisms to fresher water. Distribution and abundance of subtidal meiofauna in the sediment showed the monthly faunal abundance to range from 491 to 2791/10 m<sup>2</sup> and dry weight biomass from 0.16 to 2.8 mg/10m<sup>2</sup>. Over 60% of the fauna was restricted to the top 2 cm layer of the sediment because of their intolerance to low oxygen in the underlying layer. However, deeper



penetration of nematodes and polychaetes (up to 8 cm depth) in the sediment showed that they can withstand anaerobic conditions.

## **2.2. The shelf region off Goa**

### **2.2.1. Introduction**

The coastal site was located at 15° 30' N and 73° 39' E about ~15 km off the Goa coast. This location was chosen for flux study because it offers different environmental condition from Mandovi estuary. The average depth at this site was 27 m. Unlike the estuary, this site was affected by low salinity conditions only at the surface during the monsoon. Monsoonal upwelling plays a major role in the biogeochemistry of the open coastal waters. The sediments are almost never affected by the fresh water runoff. Circulation and currents have been well studied before several authors (as given below). However seasonal variation of other parameters such as temperature, salinity, oxygen, nitrous oxide, hydrogen sulfide, nutrients and chlorophyll are presented below as observed during the studied period.

### **2.2.2. Hydrographic features**

#### **2.2.2.1. Circulation**

Due to differential solar heating across the Indian Ocean and Eurasian land mass, the Arabian Sea experiences seasonal reversal of wind which is manifested in the form of South West Monsoon from June to September and North East Monsoon from November to February. The most prominent feature of west coast of India is coastal upwelling which occurs in the southwest monsoon season (June-September) induced by off shore Ekman drift. This generally enriches the near-surface waters with nutrients over the inner and mid-shelf regions during the SW monsoon (Banse, 1968). In the region of the present study, water circulation remains less energetic and comparatively poorly organized during the southwest monsoon. The West India Coastal Current (WICC) begins to flow equatorward in March, becomes strongest by July and collapses by October (Cutler & Swallow, 1984; Shetye & Shenoi, 1988). This current spreads over ~150 km and transports 4 Sv in the south and 0.5 Sv in the north (Shetye, 1998). Because of upwelling, thermocline shoals up toward the coast. The upwelled water is generally prevented from reaching the surface by a thin warmer, low saline layer formed due to intense

precipitation in the coastal zone. Off Goa, Naik (2003) observed upsloping of thermocline between June and October. The characteristic feature of the temperature structure just off the continental margin is the upward sloping of isotherms towards the coast and downward tilt towards the bottom which is indicative of the existence of an undercurrent (Shetye *et al.*, 1990). The undercurrent can be identified by its salinity ( $< 35.40$ ) and oxygen content ( $>10 \mu\text{M}$ ). This poleward undercurrent becomes progressively less distinct from south to north (Shetye *et al.*, 1990), but still detectable at least as far as off Mumbai. Upwelling along the west coast of India begins in the south and gradually shifts northward.

During the northeast monsoon, surface circulation in the Arabian Sea is generally anticlockwise. In contrast to western Arabian Sea where the southward flow during the NEM is much less vigorous as compared to SWM, west coast of India experiences a well developed circulation in spite of weaker winds. The northward flowing WICC becomes the most prominent surface current in the entire Arabian Sea carrying almost twice as much water ( $\sim 10 \text{ Sv}$ ) as its southward flowing variant during SWM. (Shetye *et al.*, 1991). As it moves poleward it gradually narrows down from 400 km at  $10^\circ \text{ N}$  to 100 km at around  $22^\circ \text{ N}$ , forming a narrow jet with a volume transport of 7 Sv (Shetye *et al.*, 1991). The warm, low saline waters of WICC exert a major control on biogeochemical cycling in the eastern Arabian Sea. Outside the region affected by the WICC, the surface waters are cooled to  $24\text{-}26^\circ \text{ C}$  by the northeasterly continental winds leading to deep mixed layers (Naqvi *et al.*, 2003) and entrainment of water from the thermocline, a process prevented by strong thermohaline stratification in the WICC.

#### **2.2.2.2. Temperature**

Due to downwelling that occurs off the Indian west coast during the northeast monsoon, the water column was observed to be well mixed with SST  $26\text{-}27^\circ \text{ C}$  (Fig. 2.6). With increase in solar heating in the following months (March-May) vertical stratification became little more pronounced in the water column and SST attained its maximum ( $31^\circ \text{ C}$ ). Between June-October the subsurface and bottom water cooled considerably ( $22\text{-}23^\circ \text{ C}$ ) due to the upwelling of cold water from outer shelf region. However, the existence of a low saline layer over the subsurface layer (Fig. 2.6) prevented further vertical migration of this upwelled water, and the decrease in SST was not very large. After the

collapse of upwelling towards the end of October, decreasing cloud cover and increased solar radiation led to an increase in water column temperature.

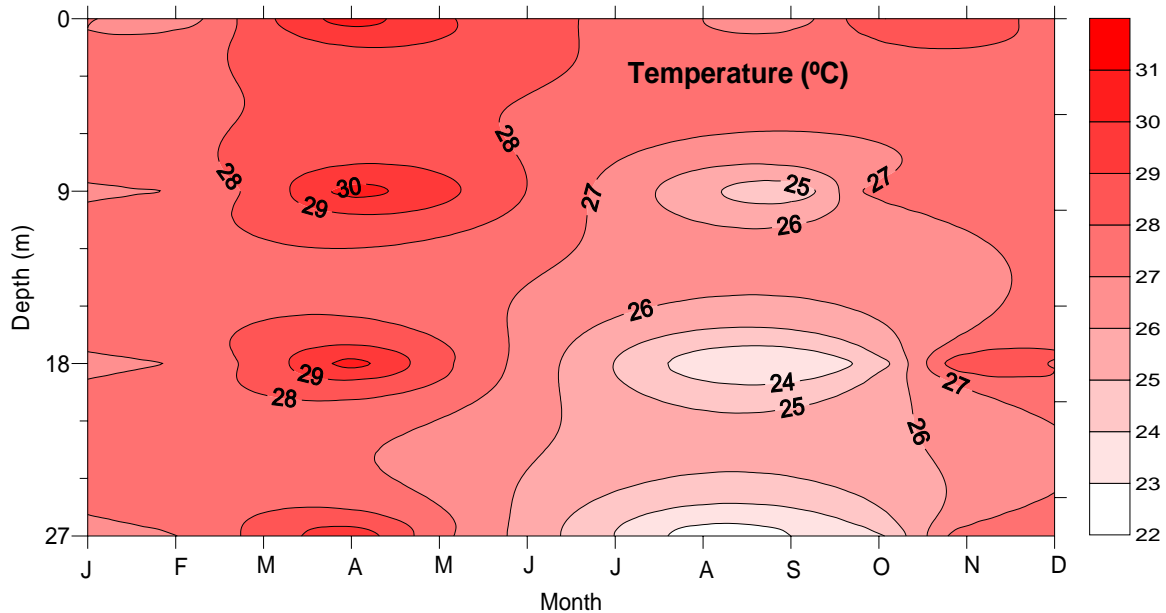


**Fig. 2.6:** Seasonal variation of temperature at the coastal station.

### 2.2.2.3. Salinity

Variation in salinity at the coastal station is within a much narrower range compared with the Mandovi estuary. In January, downwelling associated northward flow of WICC leads to non-stratified water column with salinity ranging from 35-35.1 (Fig. 2.7). However, high evaporation in the premonsoon season increases the salinity to 35.8–36.0. During the monsoon, the salinity in the subsurface layer is conspicuously lower due to the aforementioned freshening of water caused by intense rainfall in the coastal zone and larger land runoff, beneath the low saline cap lies the high- salinity upwelled water. Relatively, lower salinity throughout the water column after October is caused by the demise of upwelling and the northward transport of lower-salinity water of southern origin.

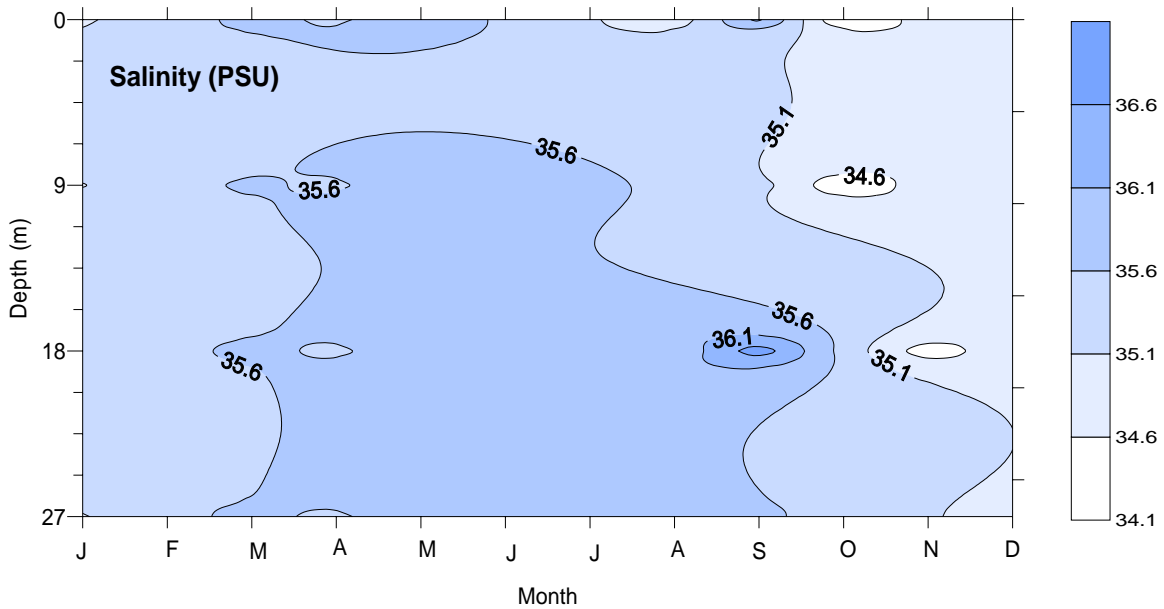


**Fig. 2.7:** Seasonal variation of salinity at the coastal station.

### 2.2.3. Biogeochemical parameters

#### 2.2.3.1. Dissolved Oxygen

Dissolved oxygen of water column is controlled by vertical mixing (or the lack of it), photosynthesis and respiration by phytoplankton. At the coastal station, oxygen concentrations are uniformly high at all depths during the northeast monsoon period (Fig. 2.8) which was because of the well mixed water column. However, as premonsoon stratification prevented vertical mixing, bottom water oxygen showed progressive decrease. In the monsoon season, suboxia developed in the subsurface water (with  $O_2 < 4\mu\text{M}$ ) because of upwelling and consumption of  $O_2$  for degradation of sinking algal detritus and poor ventilation. The reducing conditions further intensified in September-October resulting in complete anoxia ( $O_2 = 0 \mu\text{M}$ ). With the collapse of upwelling in November, dissolved oxygen again showed gradual increase which ultimately resulted in well oxygenated water column in December-January.

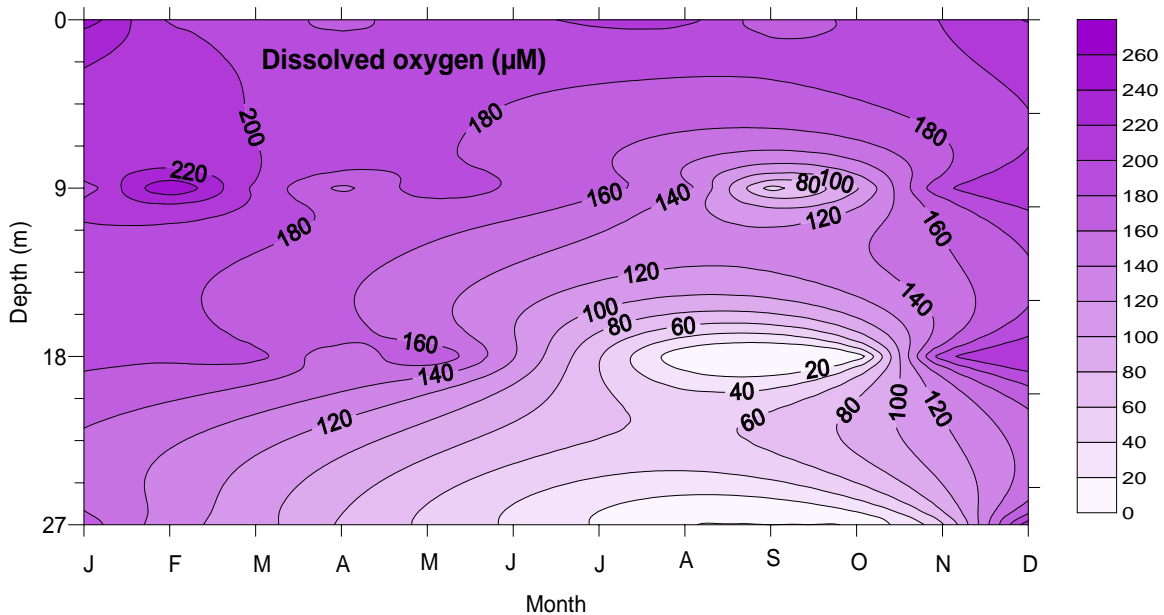


**Fig. 2.8:** Seasonal variation of dissolved oxygen at the coastal station.

#### 2.2.3.2. Nitrous Oxide

$N_2O$  is a potent greenhouse as well as an ozone depleting gas. It is produced in marine environment through both microbially-mediated nitrification and denitrification processes. In nitrification process it is produced as a byproduct whereas in denitrification process it forms as a reduced intermediate product from  $NO_2^-$ . Although  $N_2O$  is ultimately reduced to dinitrogen ( $N_2$ ) gas; it sometimes accumulates significantly owing to low  $N_2O$  reductase activity (Naqvi *et al.*, 2000).

Modest  $N_2O$  concentrations (6 -12 nM) close to or just above saturation concentration were observed from November to May. These ‘normal’ values of  $N_2O$  were observed in the water column since oxygen was well above the suboxic level. However, the onset of suboxic condition in July and August triggered vigorous denitrification which resulted in high accumulation of  $N_2O$  (~400 nM) in the subsurface and bottom layer (Fig. 2.9). This build up continued to persist even in September (~300 nM), but decreased considerably thereafter to 25 nM in October. This slower conversion of  $N_2O$  to  $N_2$  during late summer and early autumn indicates low  $N_2O$  reductase activity and higher potential of  $N_2O$  flux to the atmosphere.

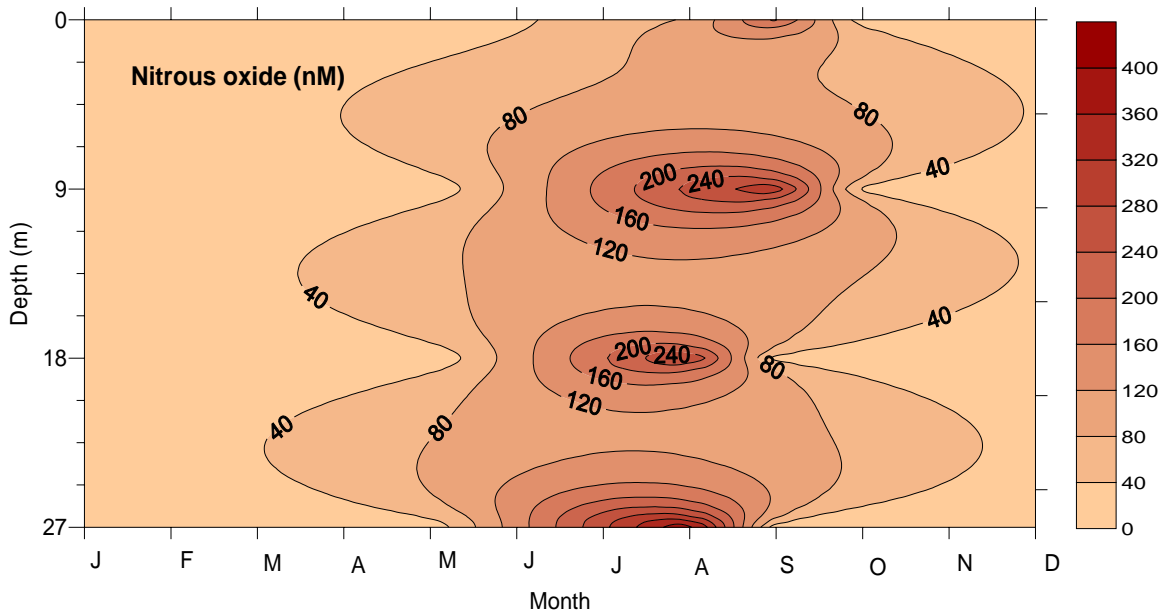


**Fig. 2.9:** Seasonal variation of N<sub>2</sub>O at the coastal station.

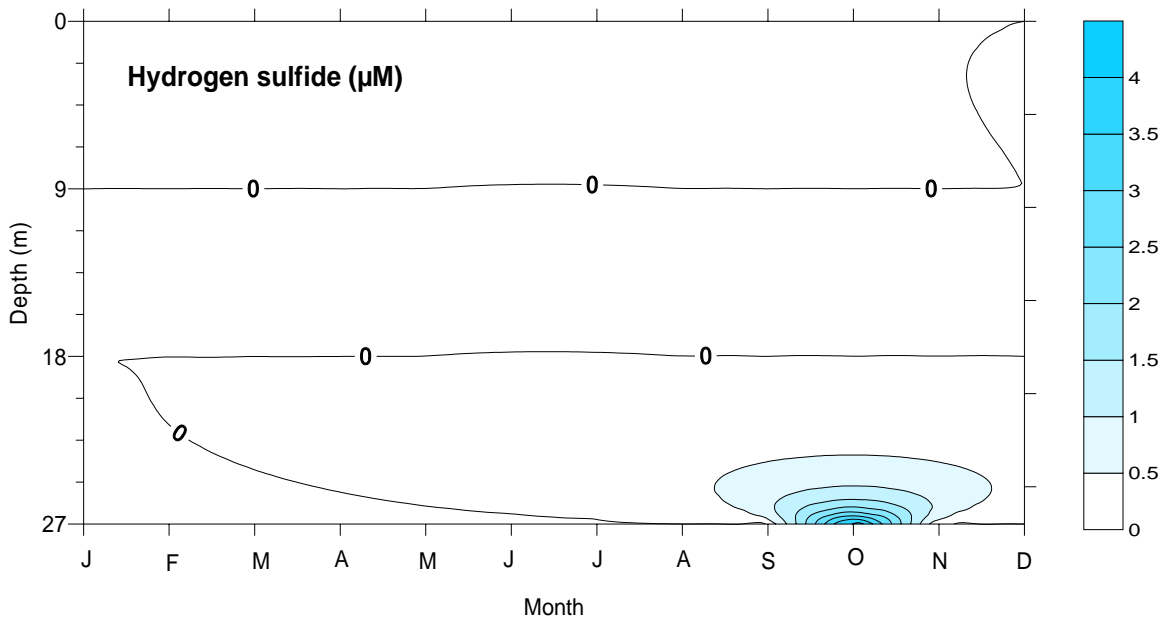


**Fig. 2.10:** Seasonal variation of H<sub>2</sub>S at the coastal station.

### 2.2.3.3. Hydrogen Sulfide

After O<sub>2</sub> and NO<sub>3</sub><sup>-</sup> are exhausted for the decomposition of organic matter, bacteria use SO<sub>4</sub><sup>2-</sup> as the terminal electron acceptor to carry out the remineralization process, resulting

in the production of  $\text{H}_2\text{S}$  and  $\text{NH}_4^+$ . Depletion of  $\text{NO}_3^-$  by September-October leads to anoxic mode of organic matter decomposition as evidenced by high accumulation of  $\text{H}_2\text{S}$  ( $4.5 \mu\text{M}$ ) in the bottom water (Fig. 2.10). However, this process ceases to occur once the oxic conditions are re-established in the water column in November.

#### **2.2.3.4. Nutrients**

The concentrations of nutrients in the water column are generally low during the northeast monsoon season. The coastal upwelling is the major process supplying new nutrients to the water column of the studied site. Enrichment of bottom water with  $\text{NO}_3^-$ ,  $\text{PO}_4^{3-}$  and  $\text{SiO}_4^{4-}$  starts in April/ May (Fig. 2.11, 2.14 & 2.15) owing to shoreward movement of nutrient - rich subsurface water from the outer shelf. While water column  $\text{PO}_4^{3-}$  and  $\text{SiO}_4^{4-}$  levels continue to be high until September/October  $\text{NO}_3^-$  concentration progressively decreases from July onwards because of onset of denitrification in the suboxic subsurface. Denitrification is at its peak in July-August which results in high accumulation of  $\text{NO}_2^-$  ( $4 \mu\text{M}$ ) in the subsurface and bottom waters (Fig. 2.12). Subsequent consumption by denitrifiers lowers  $\text{NO}_2^-$  concentration too, and by Sept-October, the water column gets almost completely devoid of both  $\text{NO}_3^-$  and  $\text{NO}_2^-$ . High accumulation of ammonium ( $10 \mu\text{M}$ ) (Fig. 2.13) and  $\text{PO}_4^{3-}$  ( $4 \mu\text{M}$ ) (Fig. 2.14) persists in the water column when the conditions are totally anoxic.  $\text{NH}_4^+$  accumulation is due to its release from organic matter mineralization via sulfate reduction. Since the regenerated  $\text{NH}_4^+$  is not oxidized under anoxic condition, it builds up. Anoxia in bottom water also causes reductive dissolution of ferric oxyhydroxide minerals (Krom & Berner, 1981) in the underlying sediment thereby releasing bound  $\text{PO}_4^{3-}$  to the overlying water.  $\text{PO}_4^{3-}$  concentrations in the subsurface water column during this period ( $>3\mu\text{M}$ ), are the highest reported yet from any part of the Indian Ocean, excluding areas greatly impacted by anthropogenic influences.

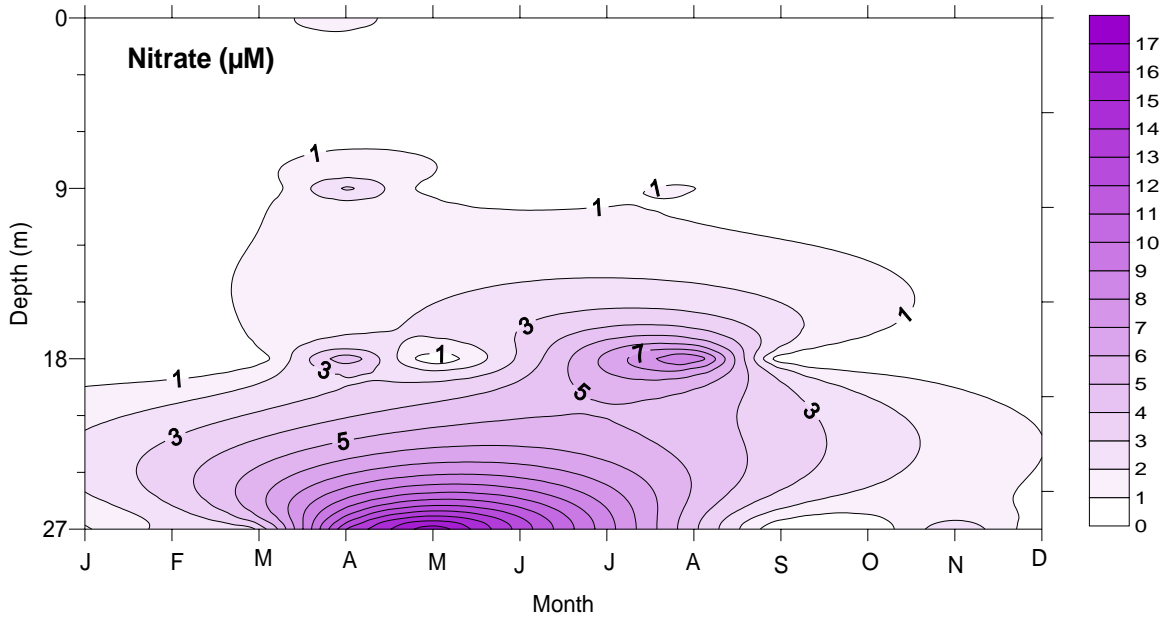


**Fig. 2.11:** Seasonal variation of  $\text{NO}_3^-$  at the coastal station.

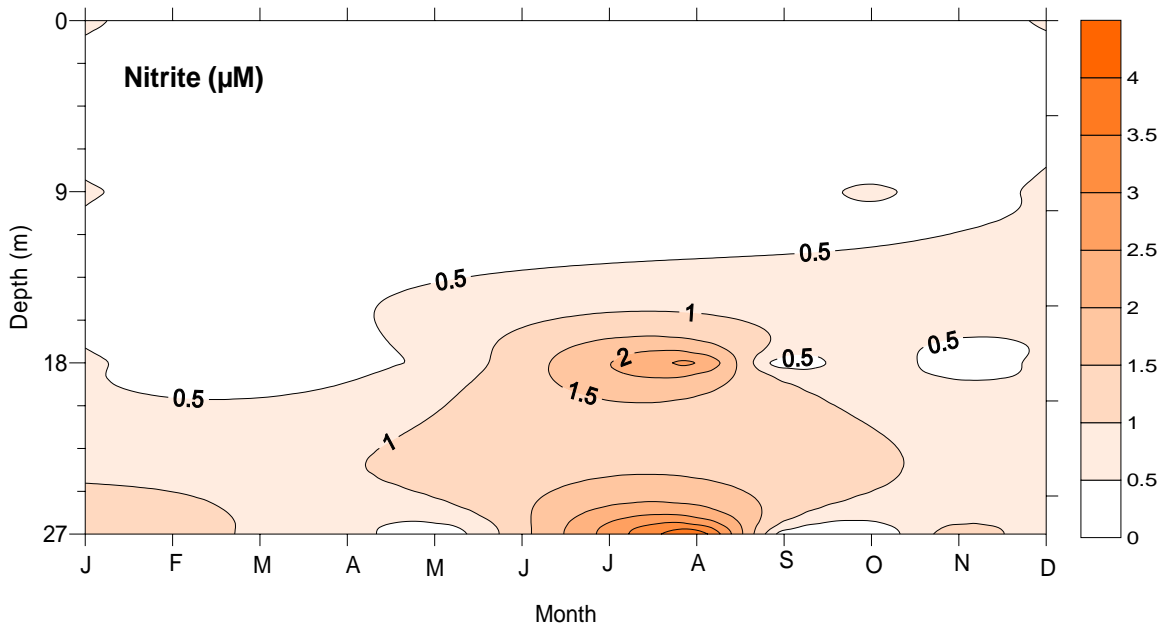


**Fig. 2.12:** Seasonal variation of  $\text{NO}_2^-$  at the coastal station.



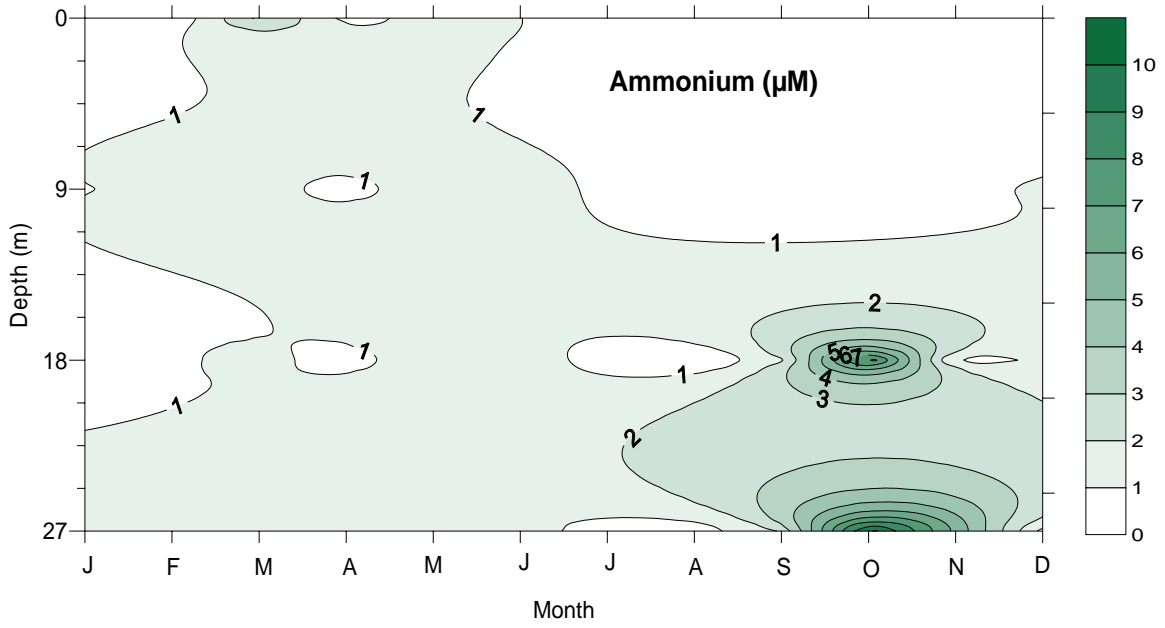


**Fig. 2.13:** Seasonal variation of  $\text{NH}_4^+$  at the coastal station.

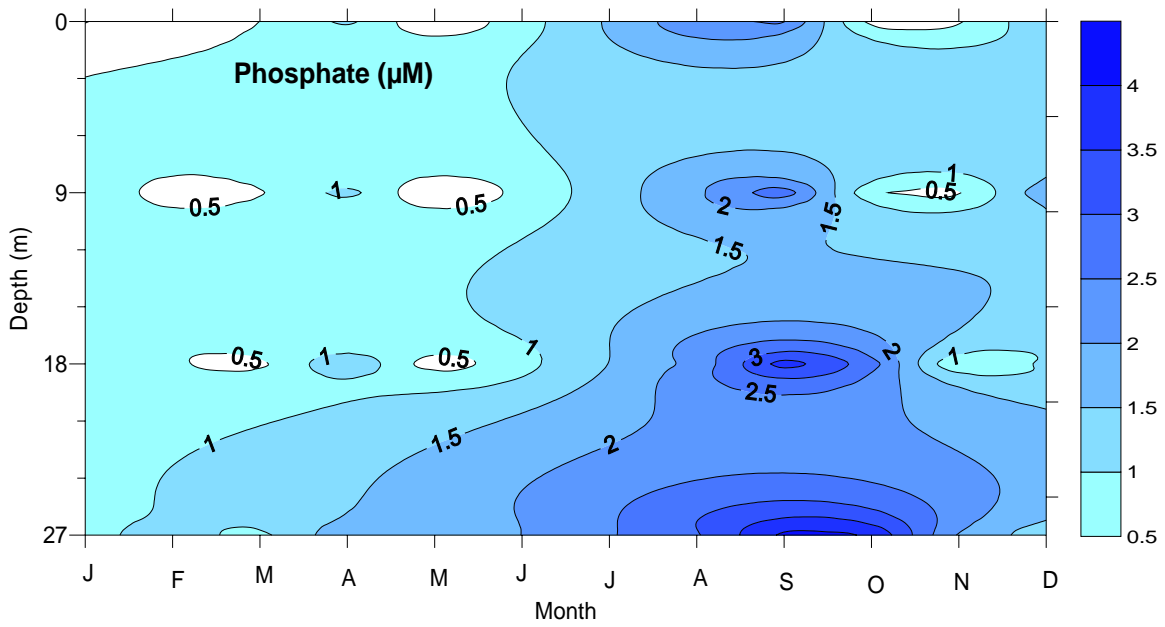


**Fig. 2.14:** Seasonal variation of  $\text{PO}_4^{3-}$  at the coastal station.

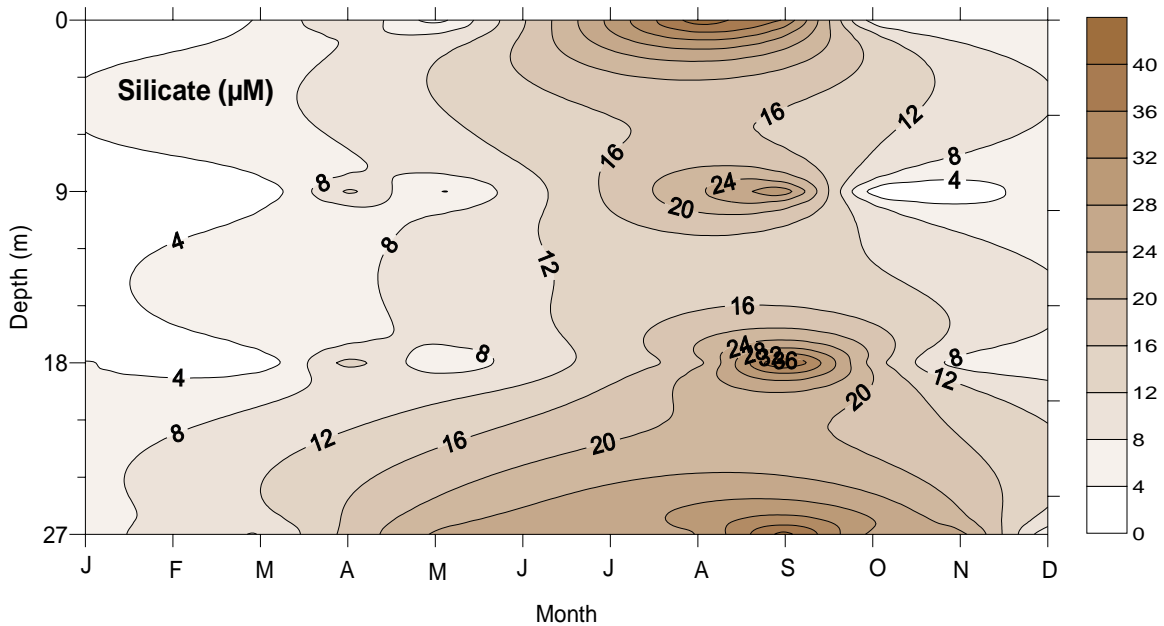


**Fig. 2.15:** Seasonal variation of  $\text{SiO}_4^{4-}$  at the coastal station.

#### 2.2.3.5. Chlorophyll and biological productivity

Chlorophyll is a measure of biomass of phytoplankton and an indicator of primary productivity. Moderate primary production occurs at the study site in the northeast monsoon season due to generally low nutrient concentrations in the water column. The productivity is comparatively higher during the premonsoon period (March-May) (Fig. 2.16) owing to increased solar radiation and nutrient enrichment through various processes. The most important of these is  $\text{N}_2$  fixation that seems to be favored by the calm weather conditions and high surface temperatures. Massive blooms of  $\text{N}_2$ -fixing *Trichodesmium* were observed during March and April in uniformity with earlier reports (Devassy *et al.*, 1978). Due to shallow depths, the new nitrogen introduced to the system by the diazotrophs is expected to be recycled, supporting other autotrophs (e.g. diatoms) and hence diverse food webs (Devassy *et al.*, 1978, Mullholland, 2006). Although *Trichodesmium* population decreases substantially later during the premonsoon due to turbulence, diatoms dominated the algal community utilizing regenerated nutrients.

Once upwelling brings nutrient-rich waters within the eutrophic zone, the biological production is expected to be greatly enhanced.

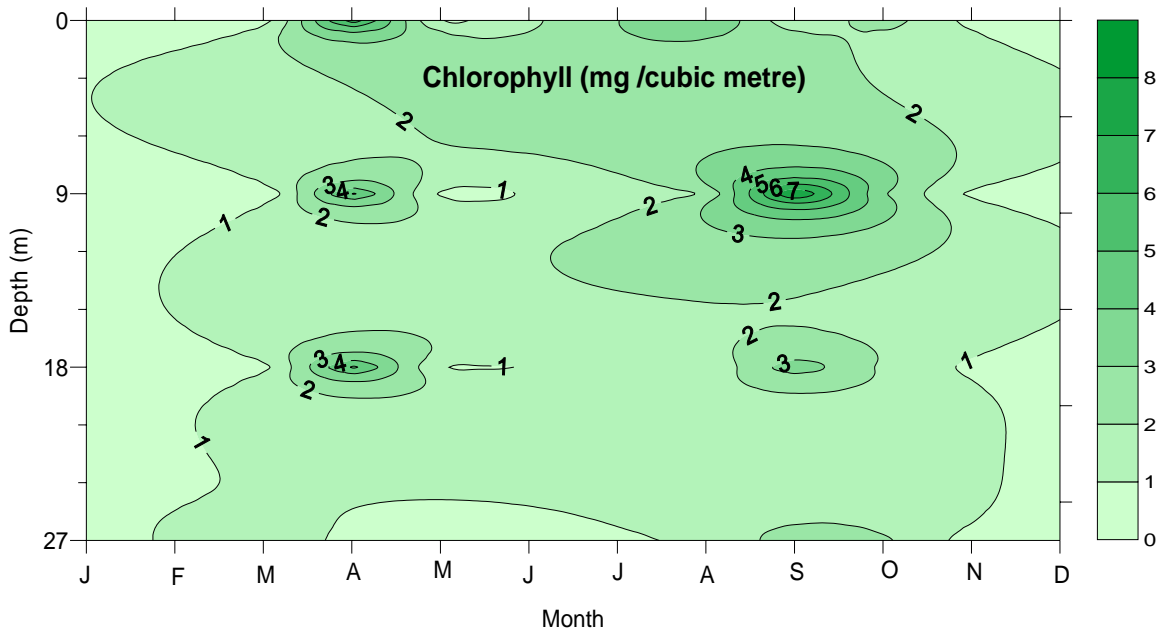


**Fig. 2.16:** Seasonal variation of Chlorophyll-*a* at the coastal station.

Four factors, however, keep primary productivity (PP) at moderate levels during the upwelling period: (1) The upwelled water is overlain by a fresher-water lens that often does not allow the former to surface. Therefore, the productivity and chlorophyll maxima are often found located a few meters below the surface (Naqvi *et al.*, 2003). (2) High cloud cover during the southwest monsoon results in decreased light penetration (*i.e.* shallow euphotic zone may not reach the nutrient rich layer). (3) Once the system becomes denitrifying, there is loss of nitrogen from the water column. The PP is thus expected to be at its minimum when the system switches over from suboxic to anoxic regimes. Once the anoxic conditions are fully established, however, nitrogen can no longer be denitrified, as it accumulates as  $\text{NH}_4^+$ . It is the availability of  $\text{NH}_4^+$  from the anoxic bottom waters to the surface layer that must determine the quality and quantity of PP during this period. (4) When the suboxic/anoxic layer extends to the euphotic zone, the phytoplankton may not be able to take advantage of the high nutrient levels because the ambient oxygen levels may be too low for them to support their own metabolic needs (Naqvi *et al.*, submitted). Thus, the processes controlling the nutrient cycling and biological production are complex and this complexity, in turn, affects the organic carbon supply and its subsequent degradation at the shallow coastal site (G5) investigated in the present study. ■

## CHAPTER - III

### MATERIALS & METHODS

#### **3.1 Introduction**

In order to meet the objectives of the present study, attempts were made (1) to cover the study area monthly for physical and biogeochemical measurements (2) to conduct incubation experiments in the field as well as laboratory. Field observations and experimental work extended from 2002 to 2007. A detailed description of sampling procedures, materials used and analytical/experimental methods adopted or developed is given below.

#### **3.2 Field Observations**

##### **3.2.1 Coastal expeditions off Goa**

Field trips were organized on a regular monthly basis to the coastal station (G5) located over the inner shelf off Goa using either NIO's research vessel *Sagar Sukti* or hired mechanized trawlers. However the observation could not be made during the early south west monsoon period because of rough seas and also a ban on boat traffic by the Captain of Ports, Government of Goa. But towards the later part of the monsoon season *i.e.* in August/September sampling could be carried out. Sampling in the estuary could be continued throughout the years without any hiatus.

##### **3.2.2 Field Experiments**

###### **(i) Benthic Chamber Experiments**

Benthic chamber experiments were carried out in the Mandovi estuary from February to August 2004. Experimental design and other details are given in *Chapter-IV*.

###### **(ii) Nutrient Enrichment Experiments**

Nutrient enrichment experiments were carried out in the estuary and at the coastal site (Stn. G5) from February to April. Details of these experiments are given in *Chapter-VI*.

### **3.3. Laboratory (Incubation) Experiments**

Sediment cores collected from the estuary and the inner shelf Stn. (G5) were incubated in the laboratory and the methodologies are described in detail in *Chapter-IV* and *Chapter-V*.

### **3.4. Methodology**

#### **3.4.1. Sampling**

Water samples were collected from selected depths covering the entire water column using Niskin samplers (5 litre capacity) manually while operating on mechanized boats (fishing trawlers), and by mechanized winch on board *Sagar Sukti*. A portable SBE CTD profiler was used for continuous profiling of water column salinity and temperature.

Despite the acquisition of temperature and salinity data by the CTD, the sharp vertical gradients in coastal and estuarine waters necessitated (the cross check) measurement of temperature for individual samples using reversible thermometer and analysis of salinity which was performed with an Autosal salinometer (Model - 8400).

Salinity samples were collected in 125 ml glass bottles that were thoroughly rinsed with the sample (3 times) and then filled up to the shoulder. The neck of the bottle was dried with a tissue paper to avoid salt deposition and consequent change in salinity. The bottles were then stoppered and stored away from heat until analysis normally completed within one month of sampling.

Samples from the Niskin bottles were first sub-sampled for dissolved gases ( $O_2$ ,  $H_2S$  and  $N_2O$ ) and then for nutrients. While sampling for dissolved gases, utmost care was taken to avoid any atmospheric contamination through bubbling. Chemical analyses of discretely- collected water samples for  $O_2$  and  $H_2S$  were done on board *Sagar Sukti*. On other field trips using trawlers, the collected samples were kept in cool dark condition after collection and chemical fixation until analyses in the institute's laboratory.

Nutrient samples were collected in plastic bottles that were rinsed well with seawater samples, filled and preserved immediately at low temperature either in an ice box (on mechanized boats) or in deep freezer (on *Sagar Sukti*) until analysis.

$N_2O$  samples were collected in 60 ml Wheaton glass bottles and immediately poisoned with saturated  $HgCl_2$  solution for subsequent analysis in the shore laboratory.

Chlorophyll samples were collected in 1 litre plastic bottles and preserved at low temperature until analyses.

At the coastal station, sediment cores were collected in a 64 mm ID acrylic liner by using a gravity corer and preserved for pore water analyses under cold and dark condition until its sectioning for pore water extraction. For the experimental purpose, cores were manually taken in a 10 cm ID PVC liner by a SCUBA diver.

In the estuary, cores were manually collected during low tide. Liners were inserted into the sediment slowly with simultaneous removal of headspace air through a syringe attached to the top cap, in order to minimize compaction of the sediment column. After collection, the cores were kept in dark and at -20 °C until further analyses.

### **3.4.2. Analysis**

#### **3.4.2.1. Dissolved Oxygen**

Standard procedures for chemical analysis were followed as per Grasshoff *et al.* (1983). Individual protocol for each constituent is briefly described below. The precision of various analysis are listed in the Table 3.1.

After fixing oxygen with the Winkler's reagents, the precipitate *i.e.*  $\text{Mn(OH)}_3$  was dissolved by acidification and the absorbance of developed colour was measured at 456 nm (Pai *et al.*, 1993) by a Shimadzu UV-visible spectrophotometer using a 1 cm cuvette. A reagent blank was also prepared by adding the acid, Winkler's B and Winkler's A solutions (in reverse order) to a volume of distilled water equal to that of the samples and the resultant absorbance at 456 nm was subtracted from the absorbance of sample. Precision of the oxygen measurement by this method is about 0.1%. This technique is particularly useful and more precise for dissolved oxygen measurements at low concentrations.

#### **3.4.2.2. Hydrogen Sulfide**

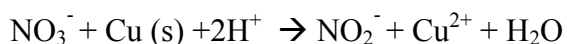
Hydrogen sulfide was determined spectrophotometrically by methylene blue method (Fonselius, 1962). The method is based on reaction of dimethyl-*p*-phenylene diamine with ferric chloride in acidic medium to form an indammonium salt (Bindshedler's green) an intermediate which in turn combines with hydrogen sulfide yielding a thiazine dye (methylene blue). This compound's maximal absorbance occurs at 670 nm.

### 3.4.2.3. *Nutrients*

Nutrients were analyzed within 24 hours of sampling. After removing from deep freezer, the water samples were allowed to attain room temperature. The samples were first analyzed together for  $\text{NO}_3^- + \text{NO}_2^-$ ,  $\text{NO}_2^-$ ,  $\text{PO}_4^{3-}$  and  $\text{SiO}_4^{4-}$ , and then separately for  $\text{NH}_4^+$  using a SKALAR *segmented flow Autoanalyzer* (Model SFA-version 4.X). The automated analyses are essentially based on the respective colorimetric methods described by Grasshoff *et al.* (1983). The primary calibration standards were prepared with utmost care and accuracy (Grasshoff *et al.*, 1983) and preserved at low temperature (4°C). The standards were compared and were found to agree well with CSK nutrient standards.

#### *Nitrite and Nitrate*

Measurement of  $\text{NO}_2^-$  involves a diazonium coupling reaction in which an aromatic amine *i.e.* N-(1-naphthyl) ethylenediamine dihydrochloride reacts with  $\text{NO}_2^-$  present in the sample to form a diazonium compound which, in turn, reacts with a secondary aromatic amine *viz.* sulphanilamide hydrochloride to form a pink coloured azo dye (Bendschneider & Robinson, 1952). The absorbance of the colour is measured at 543 nm. In case of  $\text{NO}_3^-$  the reaction mechanism, colour development and its measurement remains the same as that for  $\text{NO}_2^-$  but prior to the diazo coupling reaction, the sample is passed through a packed column of activated copperised cadmium in a buffered medium of pH 8.2 (Grasshoff, 1970) so that  $\text{NO}_3^-$  is almost quantitatively reduced to  $\text{NO}_2^-$ . The concentrations measured by this method are actually the sum of  $\text{NO}_3^-$  and  $\text{NO}_2^-$ .



Reduction of  $\text{NO}_3^-$  is very important since  $\text{NO}_3^-$  does not react with aromatic amine directly. The pH of the buffer and activity of Cd granules are important for a high yield of  $\text{NO}_3^-$  reduction. Higher pH and/or inactive metal surface leads to partial reduction of  $\text{NO}_3^-$  whereas lower pH and/or too active metal causes an over reduction of  $\text{NO}_3^-$  to NO. In both the cases,  $\text{NO}_3^-$  concentrations would be underestimated. The  $\text{NO}_3^-$  concentration is obtained by deducting  $\text{NO}_2^-$  concentration from the  $\text{NO}_3^-$  and  $\text{NO}_2^-$  concentrations.

#### *Ammonium*

Ammonium ( $\text{NH}_4^+ + \text{NH}_3$ ) reacts in a moderately alkaline (pH: 8-11.5) medium with

hypochlorite to form monochloroamine which further reacts with phenol in the presence of excess hypochlorite and catalytic amount of nitroprusside to form indophenol blue. The reaction mechanism is not yet understood completely. The ratio of phenol and active chlorine should be close to 25; otherwise appropriate colour intensity is not achieved. Citrate is added to complex Mg and Ca ions (Solorzano, 1969) which tend to precipitate at higher pH. The absorbance of the indophenol blue is measured at 630 nm.

#### *Phosphate*

Inorganic phosphate was determined by the method given by Koroleff (1963), in which phosphate is allowed to react with acidified molybdate to form a phosphomolybdate complex, which is further reduced to a blue colored complex by the addition of antimony and ascorbic acid. This blue colored complex contains Sb and P in the ratio of 1:1. Absorbance by this bluish complex is measured at 880 nm. To avoid interference from  $\text{SiO}_4^{4-}$ , pH of the final reaction was kept less than 1 and the ratio of sulphuric acid to molybdate was maintained between 2 and 3.

#### *Silicate*

Dissolved silicate in sea water was determined by making the  $\text{SiO}_4^{4-}$  in the sample react with acidified molybdate to form a yellow silicomolybdic acid. The yellow molybdic complex exists in two isomeric forms depending on pH.  $\alpha$ - isomer forms at pH 3.5-4.5 and is very stable, but  $\beta$ -isomer is less stable and forms in the pH range 2.5-0.8. After a mean reaction time of 10 min, oxalic acid was added to avoid the reaction with excess molybdate and to eliminate the influence of  $\text{PO}_4^{3-}$  present in the sample. As silicomolybdic complex is less stable in the presence of oxalic acid, ascorbic acid was added immediately to reduce the complex to a stable blue colored silicomolybdic complex. The intensity of which is measured at 810 nm. Since  $\text{SiO}_4^{4-}$  polymerizes at low temperature, samples are allowed to attain room temperature before analysis.

#### **3.4.2.4. Nitrous Oxide**

$\text{N}_2\text{O}$  was analyzed by multiple phase analysis as given by McAuliff (1971). Sample was equilibrated with equal amount of zero grade (99.999%) helium gas in a syringe. The gas in the headspace was dried over a moisture trap before injecting through a loop into a HP 5890 series II gas chromatograph. The gas mixture is then carried by the carrier flow [a mixture of argon and methane (95% Ar + 5%  $\text{CH}_4$ )].  $\text{N}_2\text{O}$  was separated from this gas



mixture by passing through a column packed with chromosorb 102 (80/100 mesh) maintained at 80°C. The separated N<sub>2</sub>O is then detected by electron capture detector (ECD, 10mCi <sup>63</sup>Ni foil conditioned at 300°C). Air (N<sub>2</sub>O = 315 ppb) was used as a working standard which was also standardized once in a while against a standard mixture of 510 ppm N<sub>2</sub>O in nitrogen gas (Gas standards, Alltech Associated Inc, IL,USA).

#### 3.4.2.5. *Chlorophyll a*

Following JGOFS protocols (UNESCO, 1994) about 500ml of seawater sample was filtered through Whatman GF/F (47 mm diameter) filter paper under low vacuum. The pigments were extracted for 24 hours in 10ml of 90% acetone in the dark in a refrigerator. Samples were measured by a flourometer at 655 nm after attaining room temperature.

#### 3.4.2.6. *Porosity*

Porosity indicates the water holding capacity of a sediment sample. To determine the porosity, the sediment sample was first weighed and again weighed after drying in oven at 100-110 °C. The difference in weight is the water content of the sediment. Then 10-20 gm of sediment sample was fully soaked with distilled water removing the entrapped air bubbles. Then it was weighed at room temperature.

Specific gravity, G can be calculated as

$$G = (W_2 - W_1) / [(W_4 - W_1) - (W_3 - W_2)]$$

Where W<sub>1</sub> = weight of the empty bottle

W<sub>2</sub> = weight of bottle with dried sediment

W<sub>3</sub> = weight of the bottle with sediment and water

W<sub>4</sub> = weight of the bottle with water

$$\text{Porosity}(\phi) = V / (1+V)$$

Where V is the void ratio and defined as follows.

$$V = G \times w$$

Where G is specific gravity and

w is the water content of the sediment which is calculated as follows.

w = wet weight of the sediment - dry weight of the sediment.

Porosity is a ratio but can also be expressed in % after multiplying with 100.

**3.4.2.7. Sedimentary Organic Carbon**

Sliced sediment layers were freeze-dried and then powdered using an agate mortar. Then they were treated with 1 N HCl to remove carbonates and subsequently washed thoroughly with deionised water and further dried. 8-12 mg of these decalcified dried sediment samples were packed in tin cups and then flash combusted with silver cobaltous cobaltic oxide and granular chromium oxide maintained at 1050 °C. Evolved CO<sub>2</sub> and NO<sub>x</sub> was then passed over a reduction column containing reduced Cu at 670 °C and were finally purified and separated with a GC at 50 °C and subsequently detected by TCD (Bhusan *et al.*, 2001). Calibration for C<sub>org</sub> was done using a Deer River shale standard containing 2.53 % C and 0.12 % N. A NCS Elemental analyzer (CE Instruments, model NCS-2500) was used for above analysis.

**3.4.2.8. Sedimentary Fe**

100 mg of dried and powdered sediments were mixed with a mixture of HNO<sub>3</sub>, HCl and HF and microwave digested. Final sample prepared in 1 N HCl was introduced into an inductively coupled atomic emission spectrometer (ICP-AES, Liberty Plasma II, Varian). Fe was measured at intensity 259.94 nm (Murray *et al.*, 2000). Calibration of the instrument was done by using multi-element standards in 0.5M HNO<sub>3</sub> of varying concentrations. Accuracy and precision of the measurement were checked by using several USGS standards e.g. SCo-1 (3.6 % Fe), MAG-1 (4.76 % Fe) and SDO-1(6.54 % Fe).

**3.4.3. Pore Water Extraction**

Sediment cores were sectioned at 1 cm interval each and filled into N<sub>2</sub> flushed centrifuge tubes inside a glove box that was continuously flushed with N<sub>2</sub>. These sediments slices were then centrifuged at 4000 rpm for 20 minutes, and the separated pore water was immediately transferred to plastic vials and kept in deep freezer at -20°C until analysis.

**3.4.4. Precision of the Methods**

Precision of the measurements were obtained by repeated calibrations and is given in the following table in terms of standard deviations (SD) and relative standard deviations (RSD).

**Table 3.1:** Precision of the methods

Sr. no.	Parameter	Method	Precision
1	Temperature	Temperature probe	$\pm 0.01^{\circ}\text{C}$
2	Salinity	Conductivity probe	$\pm 0.001$
3	Dissolved Oxygen	Winkler's titration and Spectrophotometry	$\pm 0.03 \mu\text{M}$
4	Nitrous oxide	GC-ECD	4 %
5	Hydrogen sulfide	Methylene blue method	$\pm 0.05 \mu\text{M}$
6	Nitrite	Colorimetry: Azo dye method	$\pm 0.006 \mu\text{M}$
7	Nitrate	Colorimetry: Reduction to $\text{NO}_2^-$ followed by Azo-dye method	$\pm 0.06 \mu\text{M}$
8	Ammonium	Colorimetry: Indo-phenol blue method	$\pm 0.06 \mu\text{M}$
9	Phosphate	Colorimetry: Phospho-molybdenum blue method	$\pm 0.003 \mu\text{M}$
10	Silicate	Colorimetry: Silico-molybdenum blue method	$\pm 0.01 \mu\text{M}$
11	Chlorophyll <i>a</i>	Spectrofluometry	$\pm 0.001 \text{ mg m}^{-3}$
12	Organic Carbon	GC-TCD	2 %
13	Sedimentary Fe	ICP-AES	3.64 %